

# Aeolian tones generated by a square cylinder with a splitter plate

Mohamed Sukri Mat Ali (1), Con J. Doolan (1) and Vincent Wheatley (2)

(1) School of Mechanical Engineering, The University of Adelaide, Adelaide, Australia

(2) School of Mechanical and Mining Engineering, The University of Queensland, Brisbane, Australia

**PACS:** 43.28Ra (Generation of sound by fluid flow, aerodynamic sound and turbulence).

## ABSTRACT

The generation of aeolian tones by the interaction of a low Reynolds number, low Mach number flow with a rigid square cylinder attached to a rigid thin flat plate is numerically investigated. When the length of the plate is varied from  $L = 0.5D$  to  $6D$ , where  $D$  is the side length of the square cylinder, the results can be grouped into three distinct regimes. For the first regime ( $L \lesssim D$ ), the aeolian tone levels decrease with increasing plate length. For the second regime ( $2D \lesssim L \lesssim 4D$ ), the aeolian tone levels are always higher than the single square cylinder case and they increase with increasing plate length. For the third regime ( $5D \lesssim L \lesssim 6D$ ), the levels of the aeolian tones decrease as the length of the plate increases but the levels are higher than the other regimes. These acoustic results can be explained in terms of the fluid mechanics occurring in the near wake of the cylinder.

## INTRODUCTION

Flow-induced noise is one of the engineering problems associated with bluff bodies. The noise radiated from aircraft landing gear, pantograph systems of high speed trains and the rear view mirrors of passenger cars are a few examples. This subject has received much attention (e.g.; Lockard and Lilley (2004), Hedges et al. (2002), Talotte (2000), Raghunathan et al. (2002), Kenji et al. (1999)) and is driven by consumer and government demand for a more comfortable environment.

The generation of sound sources about a rigid body immersed in a steady flow has been described theoretically by Curle (1955). Curle found that, at low Mach number, dipole sound dominates in the far-field. This dipole sound is directly related to the unsteady forces created by the fluid flow on the surface of the body.

Previous studies have shown that the unsteady forces acting on a bluff body can be controlled passively by means of wake interference (Alam et al. 2002; 2006, Prasad and Williamson 1997). For bluff bodies using a splitter plate, a non-monotonic change in Strouhal number ( $St = f \frac{D}{U_\infty}$ , where  $f$  is the vortex shedding frequency) is observed when the length of the plate is increased (Anderson and Szewczyk 1997, Kwon and Choi 1996, You et al. 1998). This is related to the different flow regimes that occur for different plate length ranges.

The changes in noise emitted by disturbed bluff body wakes are not fully understood. Available studies include the works of Leclercq and Doolan (2009), Blazewicz (2007) and Inoue et al. (2006b) for bluff bodies in a tandem arrangement, Inoue et al. (2006a) for square cylinders in a side-by-side arrangement and You et al. (1998) for a circular cylinder with a splitter plate. However, to the knowledge of the authors, there is still no available study on the case of a square cylinder with a splitter plate.

For a circular cylinder with a splitter plate, a numerical study by You et al. (1998) showed an increase in sound pressure when the

length of the plate was larger than the diameter of the cylinder. They attributed this increase to the development of a secondary vortex at the trailing edge of the splitter plate. Additionally, they found that the sound dipole from the drag fluctuations was not significant and scattering noise was substantially related to the strength of the secondary vortex.

Doolan (2008) showed that complete noise cancellation was possible by using a secondary body in the wake. Using the compact Curle's acoustic analogy, sound cancellation was possible when the two bluff bodies created the same force amplitude but were out of phase. A numerical study was then carried out for the case of a square cylinder with a detached flat plate at  $Re = 150$ . The length of the plate and its position downstream from the cylinder were set according to his theoretical analysis. A dipole sound reduction of 3.68 dB was obtained when a rigid thin flat plate was used in the wake.

The aim of this study is to investigate the sound generated by a square cylinder attached with splitter plates of various lengths. Direct numerical simulation is used to obtain a flow solution, from which unsteady acoustic source terms are extracted. An acoustic analogy based upon Curle's two-dimensional integral solution is then used to calculate sound in the acoustic far-field. The acoustic field is then described and related to the fluid mechanics in the near wake.

## TEST CASES AND NUMERICAL SIMULATIONS

Figure 1 shows a schematic diagram of the geometry investigated. A rigid square cylinder with side length of  $D$  is attached with a rigid thin flat plate (splitter plate). The thickness of the plate is fixed at  $h = 0.002D$  and its length is increased from  $L = 0.5D$  to  $6D$ . A steady free-stream flow is set over the bodies at a Reynolds number of  $Re = U_\infty D / \nu = 150$  and Mach number of  $M = U_\infty / c_0 = 0.2$ .

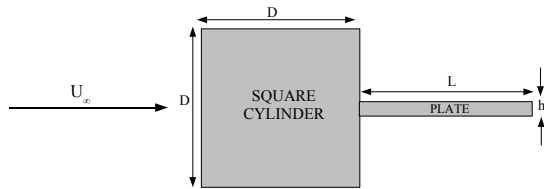


Figure 1: Sketch of the geometry investigated and annotations.

### Flow simulation

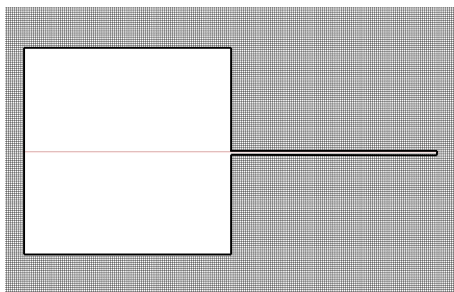
The primitive variables of the flow fields are calculated numerically based on the incompressible two-dimensional Navier Stokes equations:

$$\frac{\partial U_i}{\partial t} + U_j \frac{\partial U_i}{\partial x_j} = -\frac{1}{\rho_0} \frac{\partial p}{\partial x_i} + \frac{\partial}{\partial x_j} \left[ \nu \left( \frac{\partial U_i}{\partial x_j} + \frac{\partial U_j}{\partial x_i} \right) \right] \quad (1)$$

$$\frac{\partial U_i}{\partial x_i} = 0 \quad (2)$$

where indices  $i, j = 1, 2$  (two-dimensional) refer to the streamwise ( $x$ ) and crosswise directions ( $y$ ) in a Cartesian coordinate system, respectively. The center of the square cylinder is chosen as the origin of the Cartesian coordinates.  $U$  and  $p$  are the unsteady local velocity and pressure, respectively, at the instantaneous time of  $t$ . The OpenFOAM (Weller et al. 1998) numerical simulation system is used to solve these governing equations.

A comprehensive grid refinement study has been made and reported in Ali et al. (2009). Table 1 compares root mean square lift coefficient ( $C_{L_{rms}}$ ), mean drag coefficient ( $C_{D_{mean}}$ ) and Strouhal number ( $St$ ) from the finest grid solution of Ali et al. (2009) with the values obtained in earlier studies. A similar computational grid to the finest (case E) utilized by Ali et al. (2009) is used for the single square cylinder case in the current study. This grid has  $520 \times 440$  cells, with a finer mesh used near the cylinder such that there are 100 cells along each cylinder side. For cases of a square cylinder with a splitter plate, the computational domain is extended downstream by the plate length, so the streamwise distance between the trailing edge and the downstream end of the domain is always  $20D$ , where  $D$  is the cylinder height. As shown in figure 2, a uniform mesh with a cell size of  $0.01D$  is constructed around the splitter plate. Other grid parameters are set the same as the single square cylinder case.

Figure 2: Grid structure around a square cylinder with a splitter plate of  $L = D$ . The cells around the cylinder and the plate are uniform with a fixed size of  $0.01D \times 0.01D$ .

The 2nd-order backward scheme (Jasak 1996) is used for temporal discretisation, the convection term is discretised using

the 3rd-order QUICK scheme (Leonard 1979) and a 2nd-order central differencing scheme is used for the viscous term. The time step for pressure, convection and diffusion terms is fixed at  $\Delta t U_\infty / D = 0.002$ , which keeps the CFL number below 0.5. All analyses presented here are carried out on data sets sampled over at least 10 vortex shedding periods after statistically stationary flow is achieved. It is found that for the single square cylinder case and square cylinders with splitter plates of lengths  $L/D \leq 4.0$ , statistically stationary flow is achieved at a non-dimensional computational time of  $tU_\infty/D = 250$ . But, for a square cylinders with splitter plates of lengths  $L/D \geq 5.0$ , the flow becomes naturally unsteady after a longer computational time, and the flow is not statistically stationary until a non-dimensional computational time of  $tU_\infty/D = 500$ .

### Acoustic simulation

The propagation and fluid dynamic generation of noise is modelled using Lighthill's equation (Lighthill 1952);

$$\left( \frac{1}{c_0^2} \frac{\partial^2}{\partial t^2} - \nabla^2 \right) (c_0^2(\rho - \rho_0)) = \frac{\partial^2 T_{ij}}{\partial x_i \partial x_j} \quad (3)$$

$$T_{ij} = \rho u_i u_j - \tau_{ij} + \delta_{ij} \left( (p - p_0) - c_0^2(\rho - \rho_0) \right) \quad (4)$$

where  $\rho u_i u_j$  is Reynolds stress tensor,  $\tau_{ij}$  are the viscous stresses, and  $\rho$  and  $p$  are the instantaneous density and pressure respectively, and subscript '0' represent its respective reference value. A solution of equation (3) is found by using the two-dimensional Green's function ( $\mathbf{G}$ ) (Howe 1998);

$$\mathbf{G}(\mathbf{x}, \mathbf{y}, t - t') = \frac{\mathbf{H}(t - t' - |\mathbf{x} - \mathbf{y}|/c_0)}{2\pi \sqrt{(t - t') - |\mathbf{x} - \mathbf{y}|^2/c_0^2}} \quad (5)$$

where  $\mathbf{H}$  is the Heaviside step function,  $\mathbf{x}$  and  $\mathbf{y}$  are observer and source positions, respectively,  $t' = t - |\mathbf{x} - \mathbf{y}|/c_0$  is the retarded time and  $c_0$  is the sound speed. The two-dimensional Curle's solution of equation (3) can be re-written as:

$$c_0^2[\rho(\mathbf{x}, t) - \rho_0] = -\frac{\partial}{\partial x_i} \oint_S dl(\mathbf{y}) \int_{-\infty}^{t_i|\mathbf{x}-\mathbf{y}|/c_0} \frac{f_i(\mathbf{y}, t') dt'}{2\pi \sqrt{(t - t') - |\mathbf{x} - \mathbf{y}|^2/c_0^2}} \quad (6)$$

where  $f_i$  is the force per unit length. In this study, the propagation of sound waves in the far-field is numerically calculated based upon the acoustic analogy of Curle's integral solution (eq. (6)). In the far-field, the medium is assumed acoustically ideal and the observer location is many wavelengths distant from the near field. As the dimension of the body is very small compared to the wavelength ( $\lambda \sim 30D$ ), the two-dimensional Curle's equations (eqt. (6)) can be simplified following Inoue and Hatakeyama (2002) as:

$$p(\mathbf{x}, t) - p_\infty = p' = \frac{x_i}{2^{3/2} \pi c_0^{1/2} r^{3/2}} D(\tau) \quad (7)$$

$$D(\tau) = \int_{-\infty}^{\tau} \left[ \frac{\partial F}{\partial t'} \right] \frac{dt'}{\sqrt{\tau - t'}} \quad (8)$$

whereas  $p$  and  $p_\infty$  are localized and ambient pressure respectively,  $r$  is the observer distance from the sound source,  $\frac{\partial F}{\partial t'}$  is the time gradient of unsteady force on the body, which is obtained from the near field simulation and  $\tau = t - r/c_0$  is the retarded time. The Mach number chosen for this study is  $M = 0.2$ .

Previous studies	$C_{L_{rms}}$	$C_{D_{mean}}$	$St$
Experiments(Okajima 1982, Sohankar et al. 1999)	-	1.40	0.148 to 0.155
Doolan (2009)	0.296	1.44	0.156
Sohankar et al. (1998)	0.230	1.44	0.165
Inoue et al. (2006a)	0.40 (peak)	1.40	0.151
Ali et al. (2009)	0.285	1.47	0.160

Table 1: Comparison of the finest grid solution of Ali et al. (2009) with other previous studies

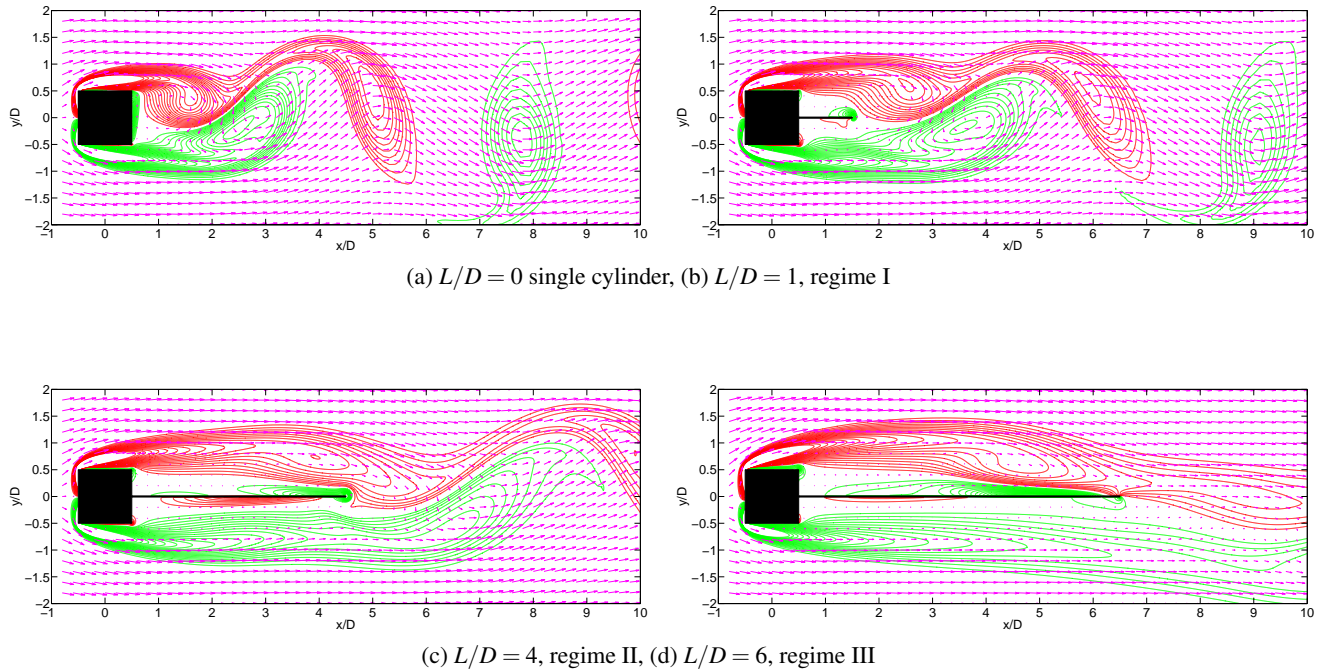


Figure 3: Vorticity contours at a time when the lift fluctuation of the bodies is maximum, coloured by direction of rotation. Red: Clockwise direction,  $-4 \leq \frac{\Omega D}{U_\infty} \leq -0.3$ ; and Green: anticlockwise,  $0.3 \leq \frac{\Omega D}{U_\infty} \leq 4.0$ . The contours are superimposed with instantaneous velocity vectors.

## RESULTS AND DISCUSSIONS

### Flow fields

The sources of noise radiated by rigid bluff bodies are related to the periodic aerodynamic forces acting on them (Curlé 1955, Inoue et al. 2006b). These periodic forces are generated due to the instability of free shear layers that induces flow oscillation, particularly in the near wake of the cylinder.

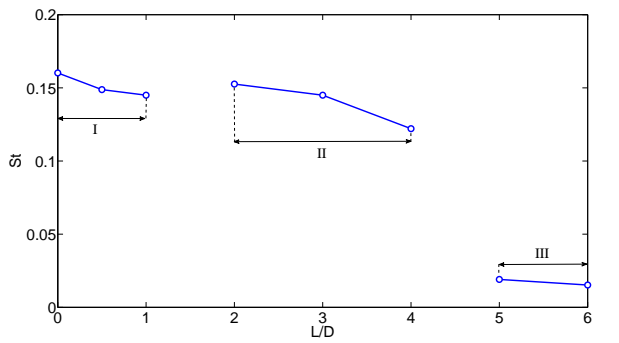
Figure 3 shows vorticity contours for a square cylinder with and without a splitter plate of various lengths. For a single square cylinder (Figure 3(a)), there is an incipient small scale vortex on the rear side of the cylinder that is generated by the face-wide vertical flow induced by the shear layers. When a splitter plate is attached to the rear side of the square cylinder, the incipient vortex is suppressed and the downstream flow structure is altered according to the plate length ranges.

For short plate lengths ( $L \lesssim D$ , regime I), the free shear layers roll-up progressively further downstream from the cylinder (i.e. Figure 3(b)) as the length of the plate is increased. Thus, the plate acts as a stabilizing mechanism, allowing the shear layers to be convected further downstream before forming large scale vortices. Consequently, a longer time is required to complete the vortex formation process. This results in a decrease in the vortex shedding frequency as the plate length is increased, as shown in figure 4a.

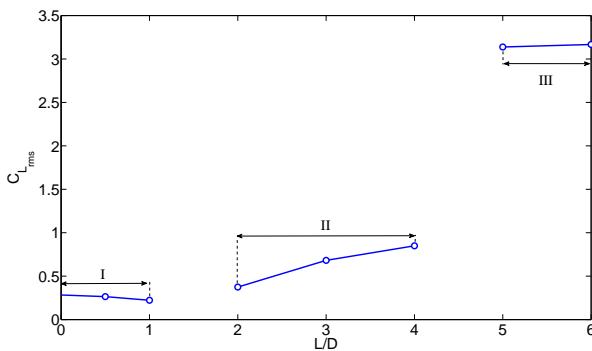
For intermediate plate lengths ( $2D \lesssim L \lesssim 4D$ , regime II), the free shear layers interact with the plate trailing edge. A strong secondary vortex is generated at the trailing edge of the plate, providing additional perturbations to the free shear layers (i.e. Figure 3(c)). Consequently the vortex shedding frequency increases between  $L = D$  and  $L = 2D$ . As the distance between the secondary vortex and the cylinder is increased, the vortex shedding frequency decreases with increasing plate length.

For long plate lengths ( $5D \lesssim L \lesssim 6D$ , regime III), the free shear layers alternately reattach to the plate (i.e. Figure 3(d)). Consequently, a markedly different flow structure is observed in this regime. The interaction between top and bottom free shear layers is suppressed by the long plate and the formation of a Kármán vortex street is prevented. However, the long shear layers are observed to oscillate in the wake. Thus, a large drop in vortex shedding frequency is detected when the length of the plate is increased from  $L = 4D$  to  $L = 5D$ .

The regimes identified earlier can also be observed in changes of the root mean square of lift fluctuations ( $C_{L_{rms}}$ ). This is shown in figure 4b. For the first regime ( $L \lesssim D$ ),  $C_{L_{rms}}$  decreases as the length of the plate is increased. However, in the second regime ( $2D \lesssim L \lesssim 4D$ ), a relatively strong secondary vortex develops at the trailing edge of the plate and amplifies the magnitude of  $C_{L_{rms}}$ . Consequently, there is an increase in  $C_{L_{rms}}$  between regime I and regime II. Then, in this latter regime,  $C_{L_{rms}}$  increases as the plate length is increased. For the third



(a) Variations of Strouhal number ( $St = f \frac{D}{U_\infty}$ , where  $f$  is vortex shedding frequency) of a single square cylinder with and without splitter plate of various lengths.



(b) Variations of root mean square lift fluctuations ( $C_{L,rms}$ ) of a single square cylinder with and without splitter plate of various lengths.

Figure 4: Strouhal number ( $St$ ) and root mean square lift fluctuations ( $C_{L,rms}$ ) for various plate lengths. Regimes I, II and III are identified according to the flow characteristics

regime ( $5D \lesssim L \lesssim 6D$ ), the reattachment of the free shear layers on the plate makes  $C_{L,rms}$  increases significantly.

## Acoustics

Figure 5 shows a comparison of sound directivities in the far-field between the two-dimensional compressible DNS analysis of Inoue et al. (2006a), which resolves the flow and far-field noise in one step, and equation (7) of the current study. Both calculations are for the case of a single square cylinder. Good agreement is obtained between the current calculation and the DNS results. The small deviation between the two lines in the upstream direction is due to the Doppler effect, which is not taken into account in this study. The maximum sound pressure level from the DNS is 37.1 dB and from equation (7) is 37.0 dB, and at directions  $\pm 105^\circ$  and  $\pm 90^\circ$ , respectively, showing excellent comparison. As the Mach number chosen ( $M = 0.2$ ) in this study only produces a small deviation from the DNS results, the Doppler effect is neglected.

Figure 6 compares sound directivities of a single circular cylinder from the numerical study of Inoue and Hatakeyama (2002) with the single square cylinder of the current study. The pattern of sound directivities for both cases is identical, which indicates a similar sound generation mechanism. The dipolar nature of the directivities shows that the unsteady lift dominates the aeolian tone level in the far-field. As the root mean square lift fluctuation at  $Re = 150$  for a circular cylinder ( $C_{L,rms,c} \sim 0.36$ , (Norberg 2003)) is larger than for a square cylinder ( $C_{L,rms,s} = 0.28$ ), the magnitude of aeolian tones for a circular cylinder (40.3 dB) are larger than for a square cylinder (37.0 dB).

Vortex shedding from the top and bottom sides of the bodies generate pressure pulses around the bodies. A negative pressure fluctuation is generated on the side of the body over which the free shear layer is being shed into the wake, whereas the opposite side experiences a positive pressure fluctuation. Figure 7 shows the instantaneous sound pressure contours of the generated aeolian tones for selected cases of a square cylinder with and without a splitter plate. The orientation of the sound pressure contours for all cases being investigated are identical, indicating a strong dependence on the same parameter, which is the lift fluctuation. The wave lengths of each case can be estimated by  $\lambda \sim \frac{D}{M \times St}$ , where  $M = \frac{U_\infty}{c_0}$  and  $St = f \frac{D}{U_\infty}$  are Mach number and the non-dimensional vortex shedding frequency, respectively. The wave lengths of the aeolian tones for regimes I and II are in the range of  $31D < \lambda < 41D$ . A very long sound wave is generated for regime III (i.e.;  $\lambda \sim 327D$ ) as a result of very low vortex shedding frequency ( $St$ ).

The frequencies of the generated aeolian tones for all cases being investigated are the same as the vortex shedding frequencies. Figure 8 shows power spectrum density analyses of the dipole sound sources calculated from equation (8) for all cases being investigated. For the single square cylinder, a tonal signal is observed at a frequency of the vortex shedding. However, when a splitter plate is attached to the rear surface of the cylinder, a secondary weak tone is observed at three times the vortex shedding frequency (the first lift harmonic). This additional tone is due to the interaction of the plate with the near wake. An interesting feature is observed for the cases in the regime III. There are a series of tones at harmonic frequencies that have decreasing amplitude with increasing frequency. This is due to the re-attachment of the free shear layers onto the plate that induces a more complicated near wake flowfield.

The directivities of root mean square pressure fluctuations ( $\tilde{P}_{rms}$ ) of the total aeolian tones at a distance of  $R = 80D$  are plotted in figure 9. It is observed that the variations in  $\tilde{P}_{rms}$  with plate length can be grouped into three patterns, that are identical to the respective regimes identified earlier. For regime I, reductions in  $C_{L,rms}$  are accompanied with reductions in the level of the aeolian tones. However, for regime II, the generated aeolian tone levels are higher than for the first flow regime and its magnitude is increased as the plate length is increased. This is due to the secondary vortex that amplifies the magnitude of  $C_{L,rms}$ , as explained in the previous section. For regime III, the generated aeolian tone levels are the strongest due to the sudden jump in  $C_{L,rms}$ . Interestingly, in this regime, when the length of the plate is increased from  $L = 5D$  to  $L = 6D$ , the magnitude of  $\tilde{P}_{rms}$  is decreased, even though the  $C_{L,rms}$  is increased. This is due to the reduction in Strouhal number as the plate length is increased, so the time gradient of the lift fluctuation for  $L = 6D$  is less than for  $L = 5D$ .

Figure 10 shows the changes in the root mean square of sound pressure ( $p'_{rms}$ ) with plate lengths at an observer location of  $R = 80D$  and  $\theta = 90^\circ$ . The optimal plate length for sound reduction is found to be  $L = D$ , where 3 dB sound reduction can be obtained. Beyond  $L = D$ , the magnitude of  $\tilde{P}_{rms}$  is larger than for the single square case. The highest sound pressure is generated by a plate with  $L = 5D$ , due to the high lift fluctuations. Thus, a splitter plate attached to the rear surface of a square cylinder is only effective as a means of noise reduction when  $L \leq D$ .

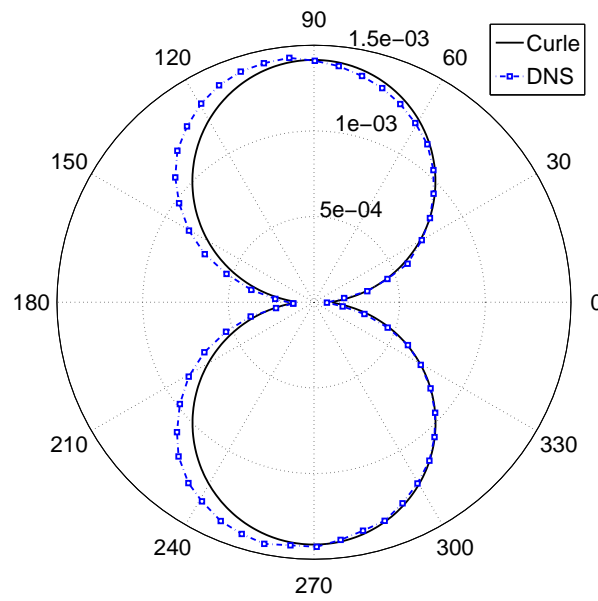


Figure 5: Comparison of directivities of root mean square sound pressure ( $\tilde{P}_{rms} = p'_{rms}/(\rho U_{\infty}^2)$ ) between DNS (Inoue et al. 2006a) and equation (7) of Curle integral solution at  $Re = 150$ ,  $M = 0.2$ ,  $S = 1$  and  $R = 75D$  for a single square cylinder.

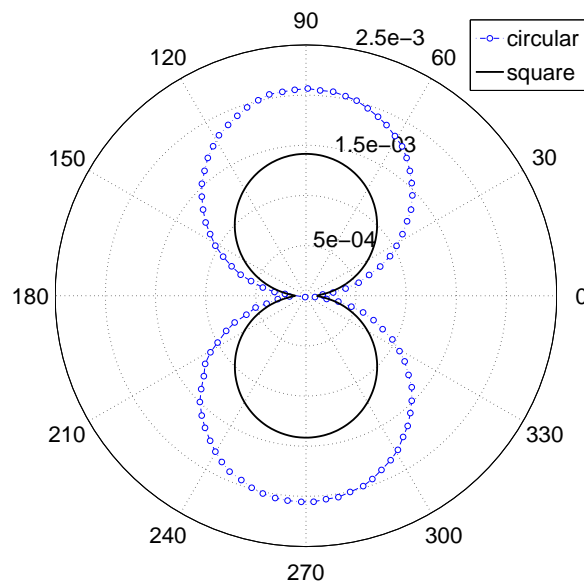


Figure 6: Comparison of directivities of root mean square sound pressure ( $\tilde{P}_{rms} = p'_{rms}/(\rho U_{\infty}^2)$ ) between circular (Inoue and Hatakeyama 2002) and square cylinders at  $Re = 150$ ,  $M = 0.2$ ,  $S = 1$  and  $R = 75D$ .

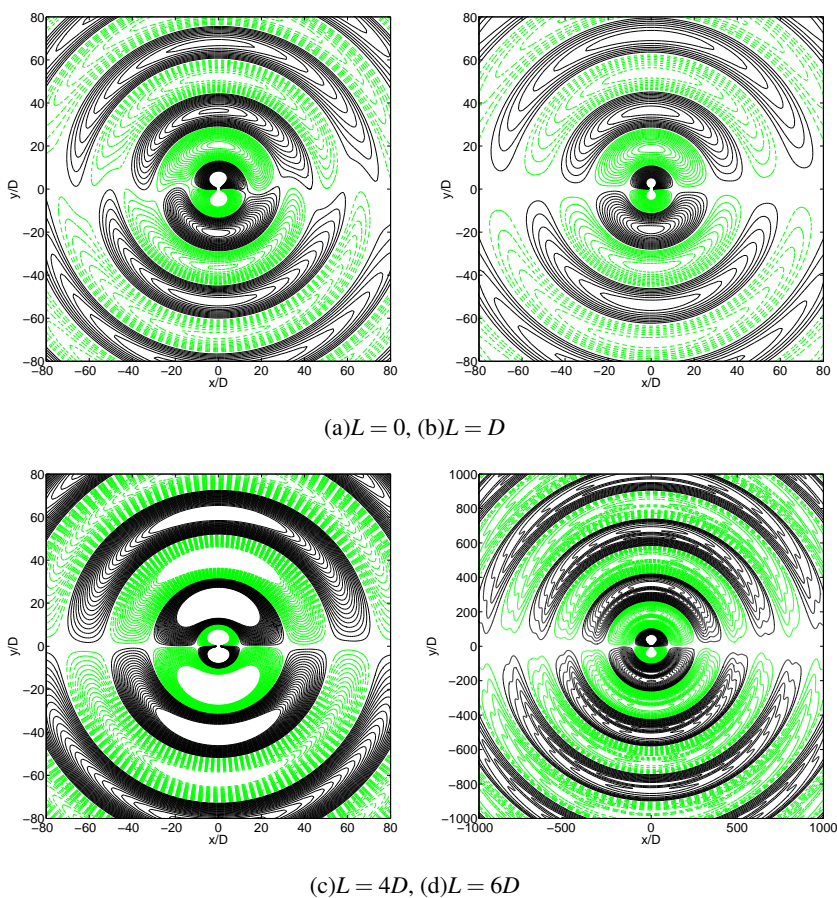


Figure 7: Contours of instantaneous acoustic pressure ( $\bar{P} = p' / (\rho U_\infty^2)$ ) at  $M = 0.2$  and  $Re = 150$ . Black solid lines represent positive sign and green dashed-lines represent negative sign. The contour levels are from  $2.0e^{-4}$  to  $5.0e^{-3}$  with a constant increment of  $2.0e^{-4}$ .

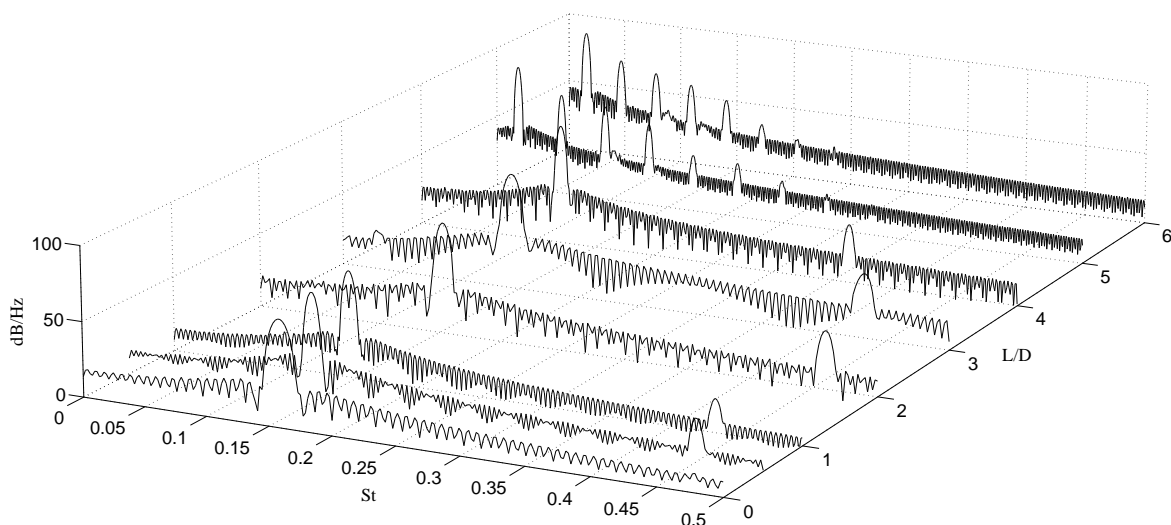


Figure 8: Sound spectra for various plate lengths.

## SUMMARY

Direct numerical simulations have been carried out to investigate the generation of aeolian tones and their propagation in the far-field for a square cylinder with and without a splitter plate. Three regimes that are dependent on the splitter plate length have been identified.

The first regime ( $L \lesssim D$ ) gives reductions in the magnitude of the aeolian tones when compared with a single square cylinder. For the second regime ( $2D \lesssim L \lesssim 4D$ ), tonal noise increases with the length of the plate. For the third regime ( $5D \lesssim L \lesssim 6D$ ), the reattachment of the free shear layers on the plate increases the lift fluctuation significantly. Thus, the magnitude of aeolian tone in this regime is the highest when compared with the other regimes.

## ACKNOWLEDGMENTS

The authors would like to acknowledge eResearchSA for allowing the use of their supercomputing facilities.

## REFERENCES

- M. M. Alam, M. Moriya, K Takai, and H Sakamoto. Suppression of fluid forces acting on two square prisms in a tandem arrangement by passive control of flow. *Journal of Fluids and Structures*, 16(8):1073–1092, 2002.
- M. M. Alam, H Sakamoto, and Y Zhou. Effect of a t-shaped plate on reduction in fluid forces on two tandem cylinders in a cross-flow. *Journal of Wind Engineering and Industrial Aerodynamics*, 94(7):525–551, 2006.
- M. S. M. Ali, C. J. Doolan, and V. Wheatley. Grid convergence study for a two-dimensional simulation of flow around a square cylinder at a low reynolds number. In *Seventh International Conference on CFD in The Minerals and Process Industries*, Melbourne, Australia, 9–11 December 2009. CSIRO.
- E. A. Anderson and A. A. Szewczyk. Effects of a splitter plate on the near wake of a circular cylinder in 2 and 3-dimensional flow configurations. *Experiments in Fluids*, 23(2):161–174, 1997.
- A. M. Blazewicz. *On the relation between fluid flow over bluff bodies and accompanying acoustic radiation*. PhD thesis, The University of Adelaide, 2007.
- N. Curle. The influence of solid boundaries upon aerodynamic sound. *Proceedings of the Royal Society of London. Series A, Mathematical and Physical Sciences*, 231(1187):505–514, 1955.
- C. J. Doolan. Bluff body noise reduction using aerodynamic interference. In *Australian Institute of Physics (AIP), 18th National Congress*, Adelaide, South Australia, 30 November - 5 December 2008.
- C. J. Doolan. Flat-plate interaction with the near wake of a square cylinder. *AIAA Journal*, 47:475–478, 2009.
- L. S. Hedges, A. K. Travin, and P. R. Spalart. Detached-eddy simulations over a simplified landing gear. *Journal of Fluids Engineering*, 124(2):413–423, 2002.
- M. S. Howe. *Acoustics of fluid structure interactions*. Cambridge University Press, 1998.
- O. Inoue and N. Hatakeyama. Sound generation by a two-dimensional circular cylinder in a uniform flow. *Journal of Fluid Mechanics*, 471:285–314, 2002.
- O. Inoue, W. Iwakami, and N. Hatakeyama. Aeolian tones radiated from flow past two square cylinders in a side-by-side arrangement. *Physics of Fluids*, 18(4):046104, 2006a.
- O. Inoue, M. Mori, and N. Hatakeyama. Aeolian tones radiated from flow past two square cylinders in tandem. *Physics of Fluids*, 18(4):046101, 2006b.
- H. Jasak. *Error analysis and estimation for the finite volume method with applications to fluid flows*. PhD thesis, Department of Mechanical Engineering, Imperial College of Science, Technology and Medicine, June 1996.
- O. Kenji, R. Himeno, and T. Fukushima. Prediction of wind noise radiated from passenger cars and its evaluation based on auralization. *Journal of Wind Engineering and Industrial Aerodynamics*, 81(1-3):403–419, May 1999.
- K. Kwon and H. Choi. Control of laminar vortex shedding behind a circular cylinder using splitter plates. *Physics of Fluids*, 8(2):479–486, 1996.
- D.J.J. Leclercq and C.J. Doolan. The interaction of a bluff body with a vortex wake. *Journal of Fluids and Structures*, 25(5):867 – 888, 2009.
- B. P. Leonard. A stable and accurate convective modelling procedure based on quadratic upstream interpolation. *Computer Methods in Applied Mechanics and Engineering*, 19(1):59 – 98, 1979.
- M. J. Lighthill. On sound generated aerodynamically: I, general theory. *Proceedings of Royal Society London. Series A, Mathematical and Physical Sciences*, 211(1107):564–587, 1952.
- D. P. Lockard and G. M. Lilley. The airframe noise reduction challenge. *NASA Technical Report*, TM-2004-213013, 2004.
- C. Norberg. Fluctuating lift on a circular cylinder: review and new measurements. *Journal of Fluids and Structures*, 17(1):57 – 96, 2003.
- A. Okajima. Strouhal numbers of rectangular cylinders. *Journal of Fluid Mechanics*, 123:379–398, 1982.
- A. Prasad and C. H. K. Williamson. A method for the reduction of bluff body drag. *Journal of Wind Engineering and Industrial Aerodynamics*, 69-71:155–167, 1997.
- R. S. Raghunathan, H. D. Kim, and T. Setoguchi. Aerodynamics of high-speed railway train. *Progress in Aerospace Sciences*, 38(6-7):469–514, 2002.
- A. Sohankar, C. Norberg, and L. Davidson. Low-reynolds-number flow around a square cylinder at incidence: study of blockage, onset of vortex shedding and outlet boundary condition. *International Journal of Numerical Methods in Fluids*, 26(1):39–56, December 1998.
- A. Sohankar, C. Norberg, and L. Davidson. Simulation of three-dimensional flow around a square cylinder at moderate reynolds numbers. *Physics of Fluids*, 11(2):288–306, 1999. doi: 10.1063/1.869879.
- C. Talotte. Aerodynamic noise: A critical survey. *Journal of Sound and Vibration*, 231(3):549 – 562, 2000.
- H. G. Weller, G. Tabor, H. Jasak, and C. Fureby. A tensorial approach to computational continuum mechanics using object-oriented techniques. *Computer in physics*, 12:620–631, 1998.
- D. You, H. Choi, M. Choi, and Kang. S. Control of flow-induced noise behind a circular cylinder using splitter plates. *AIAA Journal*, 36(11):1961–1967, 1998.

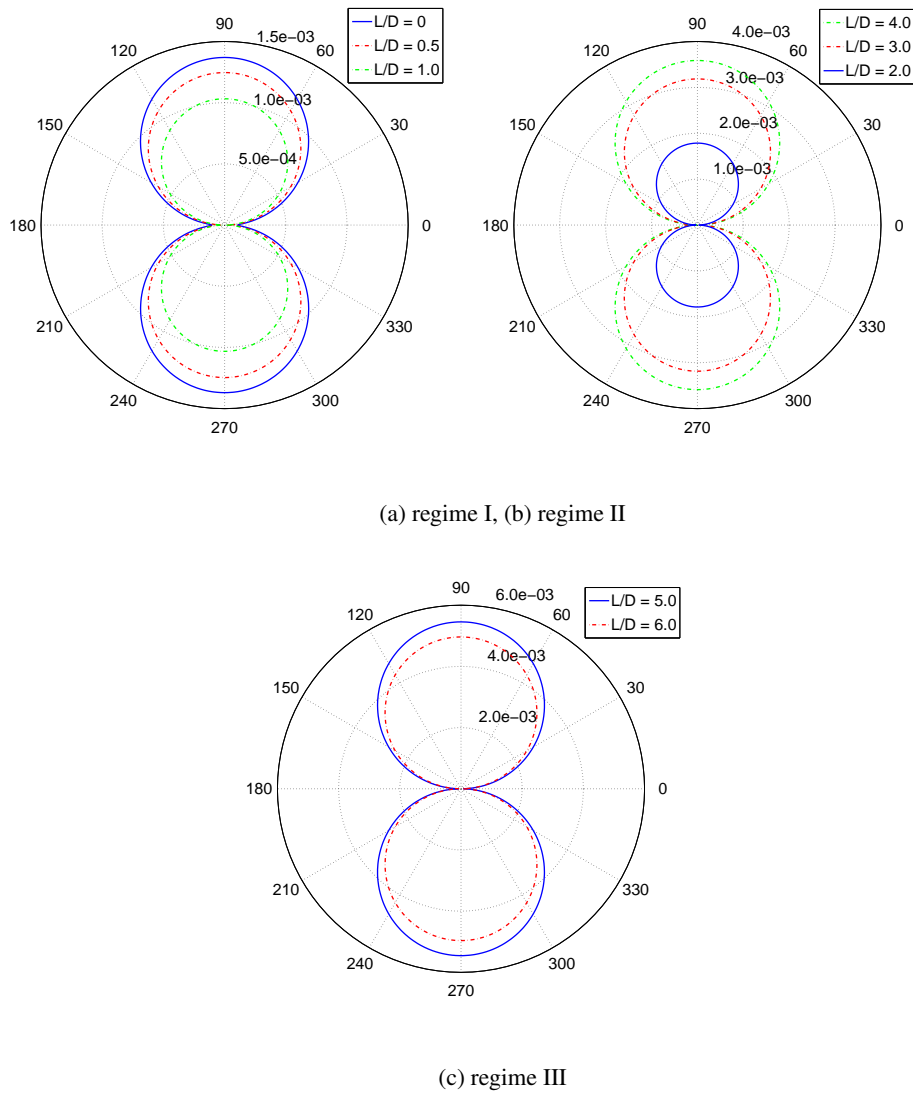


Figure 9: Sound pressure ( $\bar{P}_{rms} = p'_{rms}/(\rho U_{\infty}^2)$ ) directivities for a square cylinder with and without a splitter plate of various lengths measured at  $Re = 150$ ,  $M = 0.2$ ,  $S = 1$  and  $R = 80D$ .

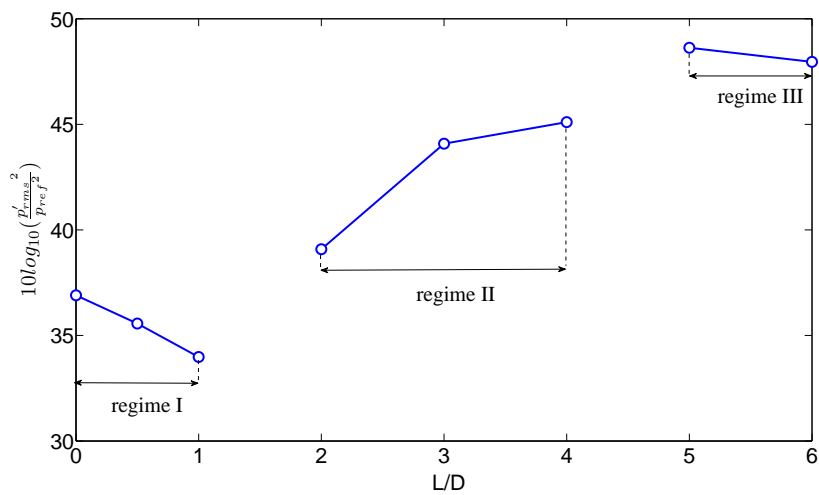


Figure 10: Variations of maximum root mean square sound pressure ( $p'_{rms}$ ) at  $Re = 150$ ,  $M = 0.2$ ,  $R = 80D$  and  $\theta = 90^\circ$  of a single square cylinder with and without splitter plate of various lengths.